

## Original Article

**Cite this article:** Eickmann B, Little CTS, Peckmann J, Taylor PD, Boyce AJ, Morgan DJ, and Bach W (2021) Shallow-marine serpentinization-derived fluid seepage in the Upper Cretaceous Qahlah Formation, United Arab Emirates. *Geological Magazine* **158**: 1561–1571. <https://doi.org/10.1017/S0016756821000121>

Received: 10 July 2020

Revised: 22 January 2021

Accepted: 11 February 2021

First published online: 18 March 2021

**Keywords:**

carbonate authigenesis; serpentinization; fluid seepage; Semail Ophiolite; United Arab Emirates

**Author for correspondence:**

Crispin T. S. Little,

Email: [c.t.s.little@earth.leeds.ac.uk](mailto:c.t.s.little@earth.leeds.ac.uk)

# Shallow-marine serpentinization-derived fluid seepage in the Upper Cretaceous Qahlah Formation, United Arab Emirates

Benjamin Eickmann<sup>1</sup>, Crispin T. S. Little<sup>2</sup> , Jörn Peckmann<sup>3</sup> , Paul D. Taylor<sup>4</sup>, Adrian J. Boyce<sup>5</sup>, Daniel J. Morgan<sup>2</sup> and Wolfgang Bach<sup>6,7</sup>

<sup>1</sup>Department of Geosciences, University of Tübingen, 72076 Tübingen, Germany; present address: Departamento de Geociencias, Universidad de los Andes, Bogotá, Colombia; <sup>2</sup>School of Earth and Environment, University of Leeds, Leeds LS2 9JT, UK; <sup>3</sup>Institute for Geology, Center for Earth System Research and Sustainability, Universität Hamburg, 20146 Hamburg, Germany; <sup>4</sup>Department of Earth Sciences, Natural History Museum, London SW7 5BD, UK; <sup>5</sup>Scottish Universities Environmental Research Centre, Scottish Enterprise Technology Park, East Kilbride G75 0QF, UK; <sup>6</sup>MARUM – Centre for Marine Environmental Sciences, University of Bremen, 28334 Bremen, Germany and <sup>7</sup>Department of Geosciences, University of Bremen, Klagenfurter Str. 2, 28359 Bremen, Germany

**Abstract**

Serpentinization of ultramafic rocks in the sea and on land leads to the generation of alkaline fluids rich in molecular hydrogen (H<sub>2</sub>) and methane (CH<sub>4</sub>) that favour the formation of carbonate mineralization, such as veins in the sub-seafloor, seafloor carbonate chimneys and terrestrial hyperalkaline spring deposits. Examples of this type of seawater–rock interaction and the formation of serpentinization-derived carbonates in a shallow-marine environment are scarce, and almost entirely lacking in the geological record. Here we present evidence for serpentinization-induced fluid seepage in shallow-marine sedimentary rocks from the Upper Cretaceous (upper Campanian to lower Maastrichtian) Qahlah Formation at Jebel Huwayyah, United Arab Emirates. The research object is a metre-scale structure (the Jebel Huwayyah Mound) formed of calcite-cemented sand grains, which formed a positive seafloor feature. The Jebel Huwayyah Mound contains numerous vertically orientated fluid conduits containing two main phases of calcite cement. We use C and O stable isotopes and elemental composition to reconstruct the fluids from which these cements precipitated and infer that the fluids consisted of variable mixtures of seawater and fluids derived from serpentinization of the underlying Semail Ophiolite. Based on their negative δ<sup>13</sup>C values, hardgrounds in the same section as the Jebel Huwayyah Mound may also have had a similar origin. The Jebel Huwayyah Mound shows that serpentinization of the Semail Ophiolite by seawater occurred very soon after obduction and marine transgression, a process that continued through to the Miocene, and, with interaction of meteoric water, up to the present day.

**1. Introduction**

Serpentinization is an exothermic geochemical reaction that takes place in marine and terrestrial settings where ultramafic rocks interact with seawater or meteoric waters, causing the hydration of the primary mafic mineralogy (e.g. olivine, pyroxenes) to serpentine, brucite and magnetite (e.g. Sleep *et al.* 2004; Bach *et al.* 2006). This process generates large quantities of hydrogen (H<sub>2</sub>), which in turn results in the formation of abiogenic methane (CH<sub>4</sub>) through the reduction of carbon dioxide (CO<sub>2</sub>) or bicarbonate (HCO<sub>3</sub><sup>-</sup>) (e.g. Proskurowski *et al.* 2008; Etiope *et al.* 2011). Fluids deriving from the reaction are enriched in hydrogen and methane, and are usually hyperalkaline (pH = 11) (Kelley *et al.* 2001; Palandri & Reed, 2004). They can also contain high concentrations of Ca from the breakdown of Ca-rich pyroxene minerals during serpentinization (Bruni *et al.* 2002; Chavagnac *et al.* 2013). When serpentinization-derived fluids come close to the seafloor or land surface, they mix with seawater or meteoric waters and carbonate minerals commonly precipitate, which are usually calcite and/or aragonite, often together with brucite (Ludwig *et al.* 2006). These authigenic carbonates can have a variety of morphologies, from veins through to highly porous chimney-like structures many metres tall (Früh-Green *et al.* 2003; Ludwig *et al.* 2006). Serpentinization-derived fluid emission has now been recognized in multiple geographic areas and tectonic settings where ultramafic rocks are exposed on land (as ophiolites) or in the sea. These include in the deep-sea, oceanic core complexes (e.g. Lost City on the Atlantic Massif; Kelley *et al.* 2001; Früh-Green *et al.* 2003), serpentinite mud volcanoes (e.g. Mariana fore-arc seamounts; Fryer *et al.* 1985) and rifted continental margins in the initial stages of ocean basin development (e.g. Iberian Margin; Agrinier *et al.* 1996; Klein *et al.* 2015). Examples also occur where ophiolites are in shallow-marine settings (e.g. Bay of

© The Author(s), 2021. Published by Cambridge University Press. This is an Open Access article, distributed under the terms of the Creative Commons Attribution licence (<http://creativecommons.org/licenses/by/4.0/>), which permits unrestricted re-use, distribution, and reproduction in any medium, provided the original work is properly cited.

**CAMBRIDGE**  
UNIVERSITY PRESS

Prony, New Caledonia and offshore Elba, Italy; Monnin *et al.* 2014; Meister *et al.* 2018), and are best known from terrestrial ophiolites (e.g. Semail Ophiolite, Oman, Del Puerto Ophiolite, California and Zambales Ophiolite, Philippines; Neal & Stanger, 1984; Abrajano *et al.* 1988; Blank *et al.* 2009; Chavagnac *et al.* 2013). Whilst serpentinization-derived fluid seepage and associated carbonate mineral formation is now well known in modern settings, direct evidence for these processes in the geological record is sparse and comes largely from carbonate veins in ophiolites, often called ophicalcites (e.g. Lavoie & Chi, 2010; Klein *et al.* 2015; Lafay *et al.* 2017; de Obeso & Kelemen, 2018, 2020; Cooperdock *et al.* 2020). Nevertheless, the process is of great interest because of the astrobiological implications of serpentinization through the abiogenic formation of organic molecules (Proskurowski *et al.* 2008; Lang *et al.* 2010).

Here we describe an ancient inferred example of shallow-marine serpentinization-related seepage in the Upper Cretaceous (upper Campanian to lower Maastrichtian) Qahlah Formation of the border region between Oman and the United Arab Emirates. We suggest that the occurrence, distribution and composition ( $\delta^{13}\text{C}$ ,  $\delta^{18}\text{O}$ , Mg/Ca, Sr/Ca, trace elements) of calcite cements in a small seafloor mound structure provides strong evidence for seepage of alkaline and methane-rich fluids that were released from the mantle section of the underlying Semail Ophiolite during the deposition of the Qahlah Formation. Associated hardgrounds in the Qahlah Formation may also have had a similar origin.

## 2. Geological setting

The Qahlah Formation crops out in the Northern Oman Mountains in the border region between Oman and the United Arab Emirates (Fig. 1a) and is the first fairly extensive sedimentary sequence to have been deposited on top of the obducted Semail Ophiolite (Smith *et al.* 1995; Alsharan & Nasir, 1996; Abdelghany, 2006; Abbasi *et al.* 2014). The age of the Semail Ophiolite is considered to be approximately coeval with the time of its obduction (Glennie *et al.* 1973), and relatively little time elapsed between the final stages of this process (Searle & Cox, 1999) and the deposition of the Qahlah Formation. The formation is time transgressive and comprises coarse clastic shallow-water sediments, variously fluvial to marine, which are difficult to date precisely, but are usually considered to be latest Campanian or early Maastrichtian in age based on the presence of rudist bivalves, corals and especially species of large benthic foraminifera such as *Loftusia* (Skelton *et al.* 1990; Smith *et al.* 1995; Abdelghany, 2006; Abbasi *et al.* 2014).

At Jebel Huwayyah, 10 km northeast of the town of Al Ain in Abu Dhabi (Fig. 1a), up to 24 m of the Qahlah Formation crops out (Fig. 1b, c). The base of the formation and its presumed contact with the underlying Semail Ophiolite are not exposed here, but at other localities to the north, Qahlah Formation sediments lie directly on top of weathered ophiolitic rocks. The Qahlah Formation at Jebel Huwayyah consists predominantly of coarse clastic sediments (conglomerates and sandstones), sometimes cross-bedded. Unlike at most other localities, the Qahlah Formation sediments at Jebel Huwayyah have an appreciable carbonate content, including thin fringing calcite cement layers on some chert cobbles, laterally discontinuous hardgrounds formed by syndepositional lithification in the lower and middle part of the section (Beds 2, 7 and 9 of Smith *et al.* 1995) and marls rich in *Loftusia* species and other large benthic foraminifera in the upper part of the section (Smith *et al.* 1995; Alsharan & Nasir,

1996; Wilson & Taylor, 2001; Abdelghany, 2006). Abdelghany (2006) interpreted the part of the Jebel Huwayyah section below the *Loftusia* beds as being deposited in fluvial to beach environments, but this seems to contradict the finding by Smith *et al.* (1995) of rare shell lenses of the marine oyster *Acutostrea* in the basal Beds 1 and 3, and rudist fragments and pebbles encrusted with *Acutostrea*, bryozoans and corals in Bed 7, suggesting rather that the entire lower part of the section has a shallow-marine origin. Within Bed 2 of the Jebel Huwayyah section is a mound-shaped structure with distinctive carbonate cement-filled vugs and tubular structures (Fig. 1d, e) that is the subject of this study, which we here call the Jebel Huwayyah Mound (JHM).

## 3. Methods

For petrographic studies, four polished thin-sections were made of the JHM matrix sediments and tubular structures, and two Qahlah Formation hardground specimens from Bed 2. These were viewed and photographed with light microscopes at Leeds University and MARUM. Subsequently, selected polished thin-sections were stained with Feigl's solution, Alizarin Red-S and potassium ferricyanide for identification of carbonate minerals. In addition, one unstained polished thin-section from the JHM was carbon coated and viewed with a Cameca SX-50 microprobe at Leeds University. Another thin-section was examined using a Zeiss Supra30 field emission gun scanning electron microscope (FEG-SEM) at the University of Bremen.

A number of distinctive carbonate cement phases were identified during the petrographic studies of the JHM tubular structures and, together with the matrix sediments and the hardgrounds, these were micro-drilled for C and O stable isotope analyses.  $\text{CO}_2$  for isotopic analysis was quantitatively released from carbonate samples by the standard procedure of overnight reaction in a vacuum with 100 % phosphoric acid at 100 °C. Gases were then analysed on a VG SIRA 10 mass spectrometer at the Scottish Universities Environmental Research Centre, monitoring mass: charge ratios 44, 45 and 46. Analytical raw data were corrected using standard procedures (Craig, 1957). All isotope data are reported in the standard  $\delta$ -notation in ‰ relative to Vienna Pee Dee Belemnite (V-PDB). The error of reproducibility, based on complete analysis of internal standards (including acid digestion) was  $\pm 0.1$  ‰ for  $\delta^{13}\text{C}$  and  $\pm 0.2$  ‰ for  $\delta^{18}\text{O}$  values. Formation temperatures were calculated after Kim & O'Neil (1997).

Minor (Mg, Si, K, Mn, Fe and Sr) and trace (Cr, Ni, Y, La, Ce, Nd, Sm, Eu, Gd, Dy, Er, Yb and Pb) elemental compositions of carbonate minerals were analysed from four polished thin-sections of the JHM with a NewWave UP193 solid state laser ablation system ( $\lambda = 193$  nm) coupled to a ThermoFinnigan Element 2 sector field inductively coupled plasma mass spectrometer (ICP-MS) at the Department of Geosciences, University of Bremen. In order to avoid surface contamination, each sample was pre-ablated five times with a spot size of 120  $\mu\text{m}$ . Carbonate samples were ablated by a laser beam (irradiance of  $\sim 0.14$  GW/cm<sup>2</sup>) with a pulse rate of 5 Hz and a spot size of 100  $\mu\text{m}$ . Data were calibrated against the NIST SRM 612 glass standard reference (Pearce *et al.* 1997) using  $^{43}\text{Ca}$  as the internal standard and assuming a Ca concentration of 40.04 wt % for calcite. Multiple laser analyses of individual calcite samples revealed a standard reproducibility of <5.5 %.

For reconstructing the past fluid Mg/Ca and Sr/Ca ratios from the JHM carbonate-filled tubes, we used the same approach as Rausch *et al.* (2013). In brief, we used an average formation temperature for the various carbonate cement phases using the

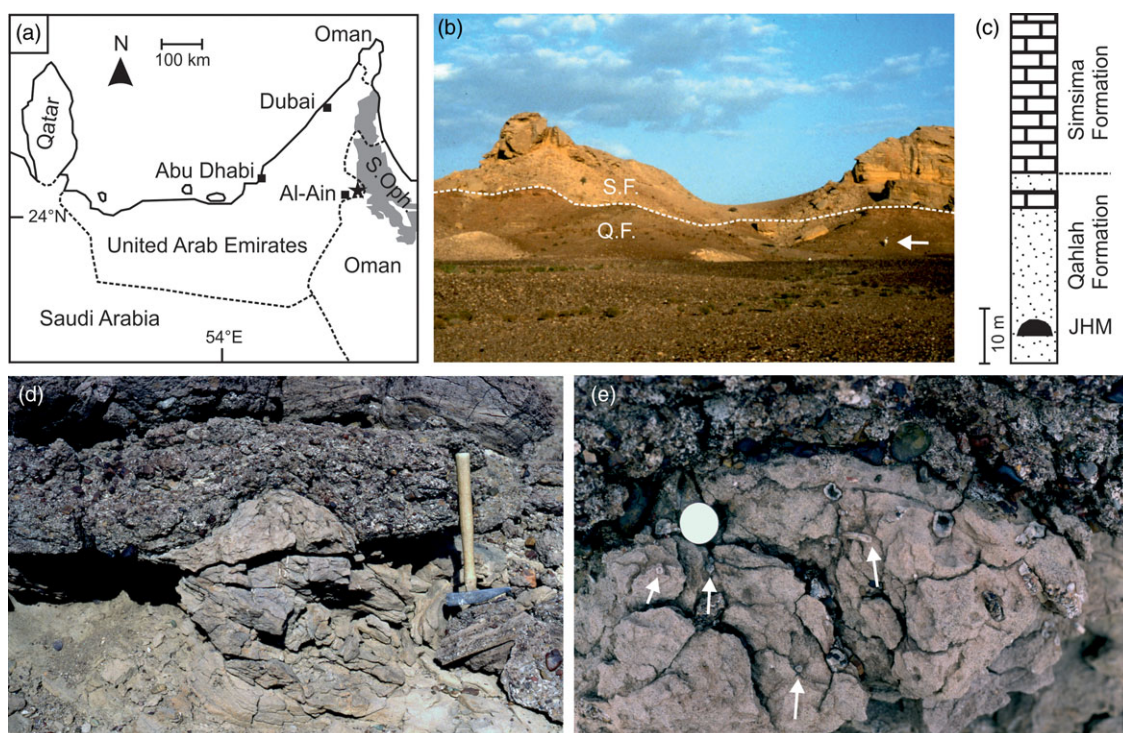


**Fig. 1.** (Colour online) (a) Location map of the Jebel Huwayyah section (black star) near Al Ain, United Arab Emirates. S. Oph. – Semail ophiolite. (b) Field image of the Qahlah (Q.F.) and the Simsima formations (S.F.) at the Jebel Huwayyah section. White arrow indicates person for scale. (c) Simplified stratigraphic section at Jebel Huwayyah showing position of the Jebel Huwayyah Mound (JHM) in lower part of the Qahlah Formation (modified from fig. 8. in Smith *et al.* 1995). Stipple pattern – predominantly sandstones and conglomerates; brick pattern – predominantly bioclastic packstones. (d) Lateral view of JHM showing lower part of structure originating in underlying bed of medium-grained sandstone and upper part draped by overlying conglomerates. Hammer for scale = 50 cm. (e) Plan view detail of exposed top surface of the JHM showing hollow vugs and tops of vertical tubular structures (white arrows). White circle centre right of image is coin (overexposed), 25 mm in diameter.

equation of Friedmann & O'Neil (1977), and the  $\delta^{18}\text{O}$  value of past seawater of  $-1\text{‰}$  for samples older than 15 million years (Muehlenbachs, 1998). The distribution coefficients for Mg/Ca were calculated after Rimstidt *et al.* (1998), whereas those for Sr/Ca were calculated as in Rausch *et al.* (2013).

## 4. Results

### 4.a. Sedimentology and petrography

The JHM is a partially eroded, roughly spherical structure  $\sim 1$  m in diameter and is formed of medium-grained lithic sandstone cemented by inclusion-rich calcite (Fig. 1d, e). The mound originates from an underlying bed of sandstone, forming a positive structure draped by overlying conglomerates (Fig. 1d). The sand grains forming the JHM are sub-angular to sub-rounded in shape and are a mixture of lithologies (Figs 2, 3), including in order of decreasing abundance: haematite-stained serpentinite, quartz, opaque chert (sometimes with radiolarian fossils; Fig. 2b, c), magnetite, chromium spinel, biotite and micritized biogenic carbonate grains (Fig. 2d). Numerous hollow vugs and tubular structures occur within the JHM, but are not found in the underlying or host sandstone, or the overlying conglomerates (Fig. 1e). The tubes are roughly cylindrical, 0.5 to 7 mm in diameter (Fig. 3), and have an orientation that is roughly perpendicular to the base of the mound (Fig. 1e). The tubes have a visible length of up to 80 mm, but because of the eroded nature of the JHM some could have originally been longer. One tube cut longitudinally has a flat base containing a small number of significantly larger fresh serpentinite grains (up to 2 mm in length), and below this base, a number of

converging, thin calcite-filled channels (Fig. 2a). This tube also shows a distinctive orientation of the surrounding sand grains, which over the space of a few millimetres become increasingly rotated towards the tube, so that some grains come to lie parallel with the tube wall (Fig. 2a). The vugs and tubes in the JHM are lined by two main phases of calcite cement: (1) an early inclusion-rich, fibrous calcite that forms isopachous rims 0.2–0.3 mm in thickness lining tube walls, which we hereafter refer to as early cement, and (2) a later phase of inclusion-free equant, blocky calcite, which we hereafter refer to as late cement (Figs 2a, 3). The early cement we interpret to be the same calcite generation that cements the grains forming the mound (Fig. 2b–d) on the basis of appearance, continuity from grain-cementing to isopachous rims (Fig. 2a) and stable isotope values (Table 1). In some tubes the late cement reveals patches of microsparitic calcite (Fig. 2a), and in some of the larger diameter tubes and vugs the late cement does not entirely fill their interiors, leaving hollow spaces (Figs 1e, 3a).

### 4.b. Carbon ( $\delta^{13}\text{C}$ ) and oxygen ( $\delta^{18}\text{O}$ ) stable isotopes

The  $\delta^{13}\text{C}$  values of the early cement in the JHM tubes range from  $-4.2\text{‰}$  to  $-3.3\text{‰}$  ( $n = 4$ ), whereas the  $\delta^{13}\text{C}$  values of the late cement range from  $-7.9\text{‰}$  to  $-5.3\text{‰}$  ( $n = 9$ ; Table 1; Fig. 4). A single  $\delta^{13}\text{C}$  value from the microsparitic cement ( $-5.8\text{‰}$ ) is similar to the range of the late cement with which it is associated. The  $\delta^{13}\text{C}$  values of the calcite cementing the grains forming the mound are between  $-3.5\text{‰}$  and  $-3.3\text{‰}$  ( $n = 3$ ). The  $\delta^{18}\text{O}$  values fall between  $-3.1\text{‰}$  and  $-1.3\text{‰}$  for the early calcite cement, between  $-3.1\text{‰}$  and  $-1.1\text{‰}$  for the late cement, and between  $-3.0\text{‰}$  and  $-2.2\text{‰}$

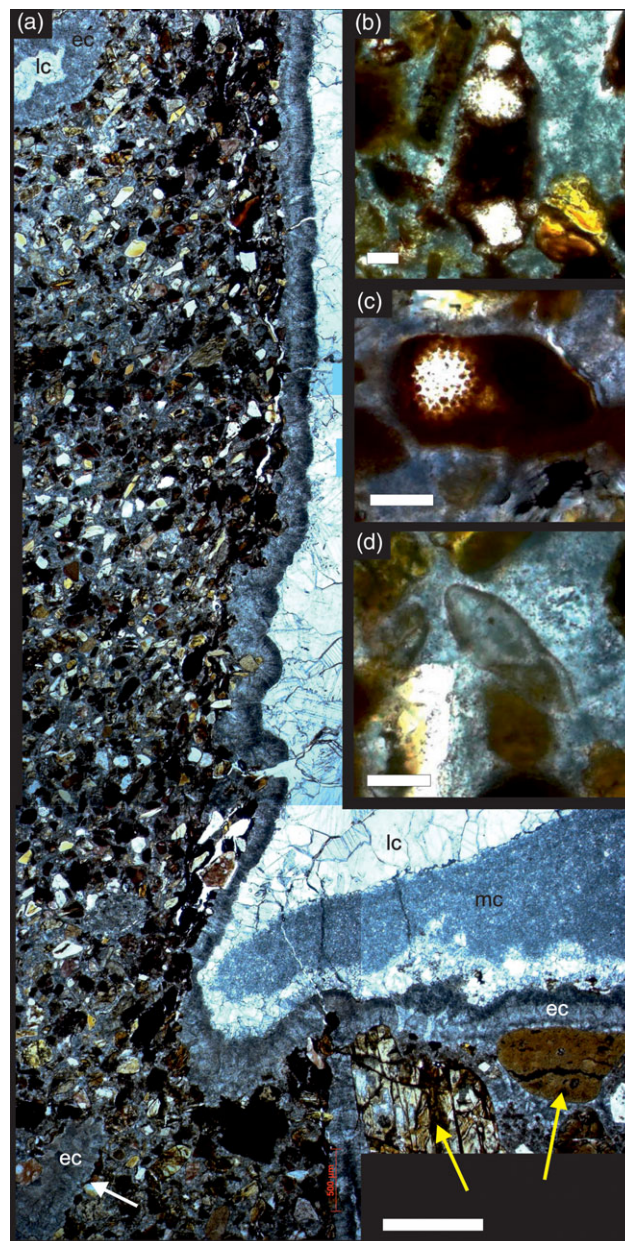


**Fig. 2.** (Colour online) Photomicrographs of petrographic thin-sections from the Jebel Huwayyah Mound (all in plane polarized light). (a) Longitudinal section through one of the fluid conduits, top uppermost in the image. At the base of the conduit are two large, fresh serpentine grains (yellow arrows) and a calcite-filled channel (white arrow). Abbreviations: ec – early cement; mc – microsparitic cement; lc – late cement. (b, c) Two opaque chert grains containing radiolarian fossils. (d) Micritized foraminiferan test. Scale bars: (a) = 500  $\mu\text{m}$ ; (b–d) = 100  $\mu\text{m}$ .

for calcite cementing the mound; one sample of microsparitic cement yielded a  $\delta^{18}\text{O}$  value of  $-1.5\text{‰}$ . The  $\delta^{13}\text{C}$  values of the Qahlah Formation hardgrounds range from  $-9.1\text{‰}$  to  $-4.8\text{‰}$ , and corresponding  $\delta^{18}\text{O}$  values are between  $-4.1\text{‰}$  and  $-0.3\text{‰}$ . The oxygen isotopic compositions were used to estimate the precipitation temperature of calcite (Table 1), using the empirical relation between  $\delta^{18}\text{O}_{\text{calcite}} - \delta^{18}\text{O}_{\text{water}}$  and temperature by Kim & O'Neil (1997).

#### 4.c. Mg/Ca and Sr/Ca ratios

The elemental composition of the calcite-filled tubular structures in the JHM reveal distinct Mg/Ca and Sr/Ca ratios for the two main cement phases (Fig. 5; online Supplementary Material Table S1).

The early cement has Mg/Ca ratios of between 9.53 and 19.44 mmol/mol and Sr/Ca ratios of 0.25 to 0.47 mmol/mol, whilst the Mg/Ca ratios for the late cement range from 0.85 to 6.45 mmol/mol and the Sr/Ca ratios are between 0.04 and 0.17 mmol/mol. The Mg/Ca and Sr/Ca ratios for the microsparitic cement are, with one exception, intermediate between the values of the early and late cements. The reconstructed Mg/Ca and Sr/Ca ratios of the parental fluid from which the calcites precipitated are listed in online Supplementary Material Table S1.

#### 4.d. Rare earth elements and yttrium

Rare earth element (REE) and yttrium (Y) concentrations of the calcite cements (Fig. 6; online Supplementary Material Table S2)

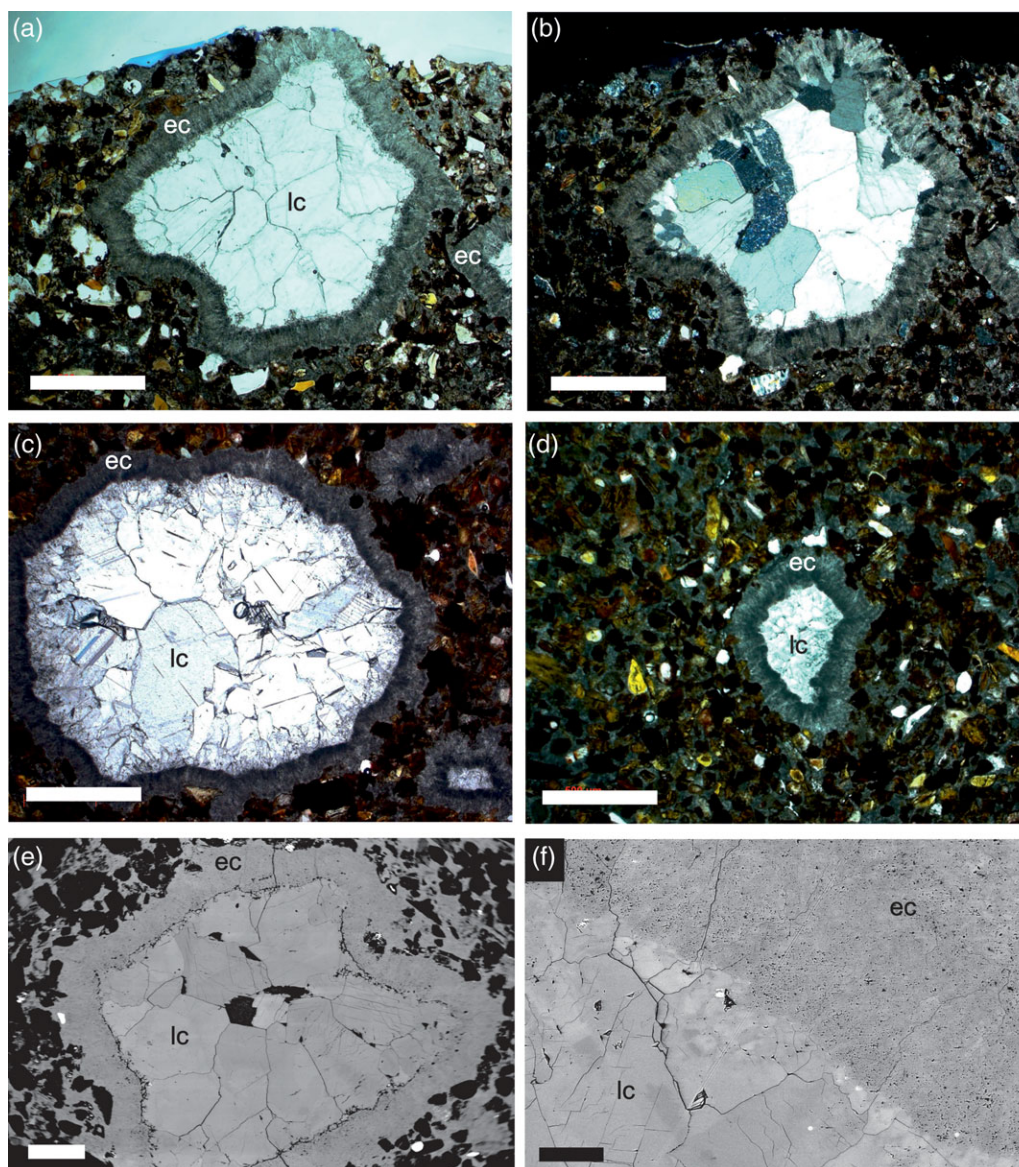


**Fig. 3.** (Colour online) Transverse sections of Jebel Huwayyah Mound fluid conduits. (a, b) Section of one conduit with particularly angular outline in (a) plane polarized light and (b) cross-polarized light. (c) Conduit with more circular outline. (d) Smaller conduit with very irregular outline. (e, f) Back-scattered electron micrographs of conduit showing late-stage cement calcite crystals increasing in size to centre of conduit and hollow interior (black space); and, (f) in detail, clear differentiation between inclusion-rich early cement and inclusion-free late cement. Abbreviations: ec – early cement; lc – late cement. Scale bars: (a–e) = 500  $\mu\text{m}$ ; (f) = 100  $\mu\text{m}$ .

show an overall flat post-Archaean Australian shale (PAAS)-normalized pattern for the late phase with small positive Y anomalies. The early cement shows slight light REE depleted patterns and lacks a positive Y anomaly. Both of the main cement phases show weak negative Ce anomalies.

## 5. Interpretations

### 5.a. Jebel Huwayyah Mound formation

The formation of the JHM began with the deposition in a shallow-marine setting of the medium-grained lithic sandstone that forms the matrix of the mound. Soon after this, on a small area of seafloor, calcite cement precipitated that bound the grains together, forming a positive mound-shaped structure. Because of the relatively low concentration of Sr in this cement phase (Fig. 5; online

Supplementary Material Table S2), we infer that the mineralogy of this early cement phase was originally calcite and not aragonite; calcite resulting from the recrystallization of aragonite tends to retain high Sr contents in the order of several thousand ppm (Buggisch & Krumm, 2005; Peckmann *et al.* 2007). We interpret the tubes within the mound to represent conduits through which the fluids flowed, from which the early-stage calcite cement precipitated. Proof of upward fluid flow comes from the rotated sand grains close to the edges of the fluid conduits and winnowed finer grains from the sediment, leaving only coarse grains in the flat bases of some of the conduits (Fig. 2a). The rims of inclusion-rich fibrous calcite (the early cement) in the vugs and tubes precipitated at the same time as the mound-forming matrix cements.

An alternative explanation for the grain rotation in the tubes might be the movement of animals through the lithic sediment to produce burrows prior to cementation. However, burrows tend

**Table 1.**  $\delta^{18}\text{O}$  and  $\delta^{13}\text{C}$  values from the Jebel Huwayyah Mound (JHM) fluid conduit cements, matrix cements and Qahlah Formation (QF) hardgrounds

Sample	Description	$\delta^{18}\text{O}$ (PDB)	$\delta^{18}\text{O}$ (SMOW)	$\delta^{13}\text{C}$ (PDB)	Formation temperature ( $^{\circ}\text{C}$ )
UAE 1-A	Early cement	-2.2	28.6	-4.2	19
UAE 2-A	Early cement	-3.1	27.8	-3.3	24
UAE 3-A	Early cement	-2.6	28.3	-3.6	21
JB4-1	Early cement	-1.3	29.6	-3.9	15
UAE 1-B	Late cement	-2.6	28.3	-5.3	21
UAE 2-B	Late cement	-3.1	27.7	-7.9	24
UAE 3-B	Late cement	-3.0	27.9	-7.2	23
UAE 2-D	Late cement	-3.0	27.9	-6.1	23
JH 2-D	Late cement	-2.8	28.1	-7.7	22
JH 2-D	Late cement	-2.7	28.1	-7.8	22
JB4-2	Late cement	-1.1	29.7	-7.0	14
JB4-3	Late cement	-1.4	29.4	-6.0	16
JB4-4	Late cement	-1.6	29.2	-6.0	17
JB4-5	Microsparitic cement	-1.5	29.3	-5.8	16
UAE 1-C	JHM matrix	-3.0	27.9	-3.5	23
UAE 2-C	JHM matrix	-2.2	28.7	-3.5	19
UAE 3-C	JHM matrix	-2.3	28.5	-3.3	20
JHH 135-A	QF hardground matrix	-1.3	29.6	-9.1	15
JHH 135-B	QF hardground matrix	-0.3	30.6	-5.4	11
JHH 135-2A	QF hardground matrix	-0.7	30.2	-4.8	12
JHH 135-2A	QF hardground matrix	-0.6	30.2	-4.9	12
JHH 135-2B	QF hardground matrix	-0.9	29.9	-4.9	14
JHH 135-2B	QF hardground matrix	-1.2	29.7	-4.9	15
JHH 135-2C	QF hardground matrix	-4.1	26.7	-7.6	29
JHH 135-2C	QF hardground matrix	-4.0	26.7	-7.6	28
JHH 146-A	QF hardground matrix	-0.5	30.4	-6.1	11
JHH 146-B	QF hardground matrix	-1.5	29.3	-6.3	16

Formation temperatures were computed from  $\delta^{18}\text{O}_{\text{SMOW}}$  values using the calibration by Kim & O'Neill (1997).

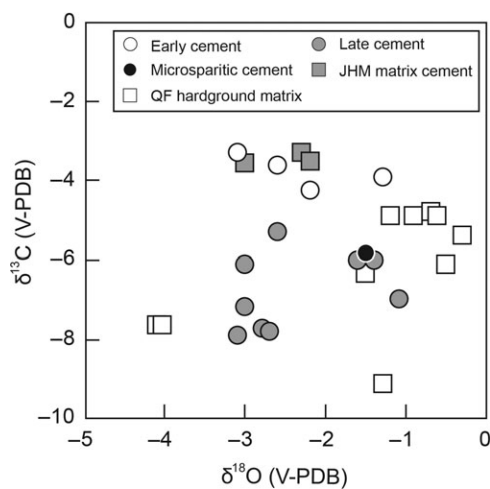


**Fig. 4.** Cross plot ( $\delta^{13}\text{C}$  v.  $\delta^{18}\text{O}$ ) of Jebel Huwayyah Mound fluid conduit cements, mound matrix and Qahlah Formation hardgrounds. Data from Table 1.

to have much more regular shapes (particularly in transverse sections) than the JHM conduits, and are almost invariably sediment filled (e.g. Bromley, 1996). The JHM tubes and vugs are also not post-cementation animal borings, because the cements and grains at the periphery of the conduit walls are not truncated, as can be seen in borings in hardgrounds and reworked cobbles higher up in the Jebel Huwayyah section (Wilson & Taylor, 2001). Plant root traces can be shaped like the JHM tubes, but again, most are filled by later sediments, and may contain carbonaceous remnants (Gregory *et al.* 2004), which the JHM conduits lack completely. In addition, animal burrows and plant root traces cannot explain the presence of vugs with the same cement linings as the tubes in the JHM, or the grain winnowing within the conduits. For these reasons we hereafter refer to the JHM tubes as fluid conduits.

Sometime after the formation of the JHM, the second phase of inclusion-free blocky calcite (the late cement) and associated microsparitic cement precipitated in the vugs and fluid conduits from later stage fluids circulating within the mound. The larger size of the late cement crystals compared to the early cement crystals

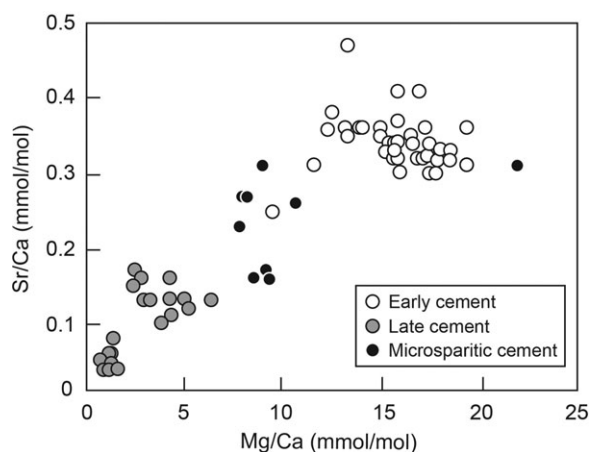


**Fig. 5.** Sr/Ca v. Mg/Ca ratios of the Jebel Huwayyah Mound fluid conduit cements. Data from online Supplementary Material Table S1.

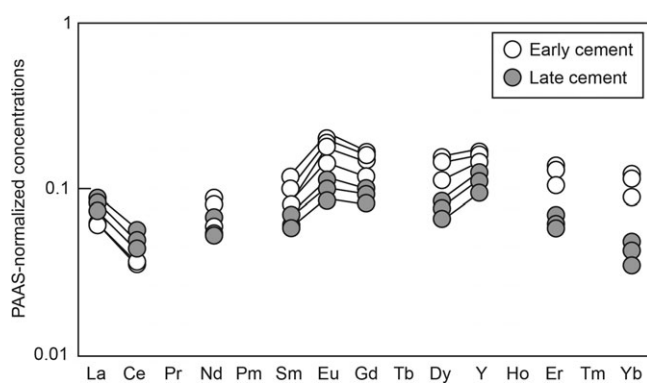


**Fig. 6.** Rare earth element and Y patterns of the Jebel Huwayyah Mound fluid conduit cements (early phase and late phase only). Data were normalized to post-Archaeoan Australian shale (PAAS; Taylor & McLennan, 1985). Note that the data presented are averages of eight to ten laser-ablation spots (see online Supplementary Material Table S2).

suggests that the precipitation of the former occurred less rapidly than the latter. The timing of the late cement formation is difficult to ascertain and most probably occurred after the JHM was covered by a layer of conglomerate and later sediments.

### 5.b. Origin and nature of the JHM cement-forming fluids

Here we use the stable isotope and element composition of the calcite cements in the JHM to reconstruct the origin and nature of the fluids from which they formed, starting with the early cement. The Mg/Ca and Sr/Ca ratios of the reconstructed parent fluid from which this cement precipitated are close or slightly lower than 1000 mmol/mol, and the corresponding Sr/Ca ratios cluster around 4 mmol/mol, respectively (online Supplementary Material Table S1). These ratios match well with the range of reconstructed Late Cretaceous seawater compositions (Mg/Ca = ~1000 mmol/mol, Sr/Ca = 2 to 6 mmol/mol) that are based on calcite veins from ocean crust in the flanks of mid-ocean ridges (Coggon *et al.* 2010; Rausch *et al.* 2013), as well as with theoretical models for the Late Cretaceous (Hardie, 1996; Wallmann, 2001). In contrast, the  $\delta^{13}\text{C}$  values (–4.2 ‰ to –3.3 ‰) from the early cement are around 5 ‰ lower than would be expected for calcite precipitated in equilibrium with dissolved

inorganic carbon (DIC) of Cretaceous seawater (+2 ‰; Wilson & Opdyke, 1996; Prokoph *et al.* 2008), and indeed the values recorded from the Maastrichtian Simsim Formation at Qalhat, NE Oman (0 to +2 ‰; Schlüter *et al.* 2008). An explanation for the negative  $\delta^{13}\text{C}$  values in the JHM early cement requires the mixing of the contemporary seawater DIC pool (modern seawater  $\delta^{13}\text{C}_{\text{DIC}} = \sim 0$  ‰; Zeebe & Wolf-Gladrow, 2001) with an isotopically lighter source of dissolved DIC. One common source of DIC with low  $\delta^{13}\text{C}$  values reflecting  $^{13}\text{C}$  depletion is the oxidation of organic carbon (Irwin *et al.* 1977). However, there is no obvious source of significant organic material (e.g. carbon-rich shales) in the sedimentary sequence hosting the JHM, as the Qalhat Formation rests directly on the crystalline rocks of the Semail Ophiolite, so another source of isotopically light DIC needs to be invoked. We suggest that the ophiolite itself could have been this source, through the production of abiogenic methane by serpentinization of peridotite. Methane in modern serpentinite-derived fluids in both the deep-sea and in ophiolite environments has negative  $\delta^{13}\text{C}$  values (–11.9 ‰ at Lost City, –10.3 ‰ at Logatchev, –16.7 ‰ at Rainbow, –18 ‰ at Elba and –7.7 ‰ in the Zambales ophiolite; Abrajano *et al.* 1990; Lilley *et al.* 1993; Charlou *et al.* 2002; Proskurowski *et al.* 2008; Meister *et al.* 2018; Sciarra *et al.* 2019). Some of this methane will be oxidized close to the seafloor to produce  $^{13}\text{C}$ -depleted DIC, and the high pH and Ca concentrations in the serpentinite-derived fluids promote carbonate precipitation on mixing with seawater (Palandri & Reed, 2004; Proskurowski *et al.* 2008). These carbonates usually (but not always) have negative  $\delta^{13}\text{C}$  values, often with the same range as the JHM cements. The abundance of serpentinite sand grains in the JHM matrix is ample evidence for serpentinization of the Semail Ophiolite to have occurred in the Jebel Huwayyah area during Late Cretaceous time, certainly prior to the formation of the sand grains, and, as we here suggest, during the deposition of the overlying Qalhat Formation.

The late cement phase precipitated from a fluid with lower Mg/Ca and Sr/Ca ratios than the early cement phase (Fig. 5). Serpentinization fluids show low Mg and high Ca concentrations relative to seawater (e.g. Kelley *et al.* 2001). Moreover, the lower Mg/Ca and Sr/Ca ratios of the JHM late cements are similar to those of serpentinite-hosted calcite from the Logatchev hydrothermal system, which Eickmann *et al.* (2009) interpreted to reflect mixing between seawater and a hydrothermal fluid. Applying this evidence to our model for the JHM, we infer that the fluids from which the late cement phase precipitated comprised a greater proportion of serpentinization-derived fluids to seawater than the early cement phase. This is corroborated by the more negative  $\delta^{13}\text{C}$  values of the late cement (Fig. 4), which indicates a greater influence of methane oxidation on the DIC pool from which this mineral phase precipitated.

Because there is a trend from higher to lower Mg/Ca and Sr/Ca ratios in carbonate cements during diagenesis (e.g. Tucker & Wright 1990; Joseph *et al.* 2013), it is possible that the JHM late cement had a diagenetic origin, from burial diagenesis and/or interaction with meteoric water during early cementation. However, this is rather unlikely for several reasons. First because the early cement and the late cement of the JHM tubes have similar  $\delta^{18}\text{O}$  values (–3.1 ‰ and –1.3 ‰ versus –3.1 ‰ and –1.1 ‰), possibly indicating that the oxygen stable isotope composition of the fluids and formation temperatures did not change much from the time when the early cement formed to the time when the late cement mostly occluded the fluid conduits. Second, we think that later diagenetic alteration would affect both the early and late JHM

cement phases, leading to homogenization of  $\delta^{13}\text{C}$  values, and Mg/Ca and Sr/Ca ratios between the early and later calcite phases. We also note that Schlüter *et al.* (2008) recorded  $\delta^{18}\text{O}$  values from the carbonate-rich Simsima Formation as low as  $-8\text{‰}$ , which they interpreted as showing diagenetic alteration; these values are considerably more negative than any found in the JHM cements.

The Mg/Ca and Sr/Ca ratios for the microsparitic cement phase are largely intermediate between the early and late cements (Fig. 5). This may indicate that the microsparitic cement precipitated from a fluid with a composition between that from which the early and late cements precipitated. However, the single  $\delta^{13}\text{C}$  value for the microsparitic cement sits in the field of the late-stage cement (Fig. 4), so it is likely the microsparitic cement precipitating fluids were more related to this later phase of cementation in the JHM.

The calculated formation temperatures for the all the JHM cement phases (Table 1) based on their  $\delta^{18}\text{O}$  values range between 14 and 24 °C (mean 19.9;  $n = 17$ ), assuming a seawater value of  $-1\text{‰}$  for an ice-free Late Cretaceous (Veizer *et al.* 1997; Prokoph *et al.* 2008). This range is at the lower end or below temperature estimates for Maastrichtian tropical sea-surface temperatures of 20 to 32 °C from planktonic foraminifera (Pearson *et al.* 2001; Zeebe, 2001), 27 to 32 °C from rudist bivalve aragonite and magnesian calcite cements (Wilson & Opdyke, 1996), and a minimum of 25 °C using the  $\text{TEX}_{86}$  proxy (Alsenz *et al.* 2013). However, these calculated JHM palaeotemperatures should be taken with caution, as we do not know the  $\delta^{18}\text{O}$  value(s) for the inferred serpentinization-derived fluids, nor the degree of mixing with contemporary seawater in the JHM during cement precipitation. Further, the cement  $\delta^{18}\text{O}$  values could have been overprinted by later diagenetic events (e.g. Tong *et al.* 2016), although see the arguments above about a possible diagenetic interpretation.

Support from PAAS-normalized REEs for our interpretation of serpentinization-derived fluids being involved in the formation of the JHM is equivocal. The REE and Y patterns of the early- and late-stage calcite cements (Fig. 6) show subtle differences between the two generations. The early cement phase displays very uniform patterns with a slight heavy REE (HREE) enrichment. The lack of a positive Y anomaly suggests that the fluid from which the early cement precipitated was modified by water–rock reactions. The late cement does show a positive Y anomaly and has lower HREE concentrations. It is not straightforward to reconcile the differences in the REE patterns with the variability in Mg/Ca ratios and  $\delta^{13}\text{C}$  values. This is in part due to the fact that REE and Y systematics of fluids involved in low-temperature serpentinization have not been investigated to date.

To sum up, we have a number of geochemical lines of evidence that the cements forming the JHM were precipitated from serpentinization-derived fluids mixed to a greater or lesser extent with Maastrichtian seawater for a period of time during the deposition of the Qahlah Formation. The formation of the JHM tubes is therefore analogous to fluid-induced chimney formation on the modern ocean floor, where the interplay between ascending venting fluids and seawater forms chimneys recording a progressive change from a seawater-like signature in the outermost part to a lesser seawater component in the inner part (Eickmann *et al.* 2014). Following from this, and with reference to the chemistry of modern serpentinization-related seeps, we infer that the JHM serpentinization-derived fluids were alkaline and rich in molecular hydrogen, abiogenic methane and Ca.

### 5.c. Qahlah Formation hardgrounds

The  $\delta^{13}\text{C}$  values of the hardground cements are similar to those of the JHM late cement, although one of the values ( $-9.1\text{‰}$ ) is the most negative of all the carbonates we measured from the Qahlah Formation (Fig. 4), and also more negative than any marine hardgrounds in the geological record documented by Erhardt *et al.* (2020), with the lowest value of  $-5.15\text{‰}$  from the Lower Cretaceous of Oman. From this we infer, again, that the fluid from which the hardground cements precipitated was not pure seawater. Although we have no supporting elemental data, we suggest that this isotopically lighter DIC source was from the same serpentinization-derived fluid that contributed to the formation of the JHM cements. Some support for this idea is that the hardgrounds are not laterally continuous (i.e. do not represent periods of basin-scale emergence or non-deposition) and are only found in the Jebel Huwayyah section, not in other outcrops of the Qahlah Formation (see Section 2). If this interpretation is correct, then it suggests serpentinization-derived fluid flow was active for a considerable time during the formation of the Qahlah Formation, but this was localized palaeogeographically to the Jebel Huwayyah area. Such localization would be expected given that sites of modern serpentine-related seepage are geographically constrained to small areas of land-based ophiolites and submarine mantle rock exposures (see Section 1).

## 6. Discussion and conclusions

There are several implications of our interpretation that serpentinization-derived fluids were involved in the formation of the JHM and conduit-filling cements, and perhaps also the Jebel Huwayyah hardgrounds. First, it expands the temporal duration of serpentinization-related seepage in the Semail Ophiolite, and the morphological diversity of resulting carbonate mineral structures. Second, it is, to the best of our knowledge, the only ancient example of a carbonate mineralized seafloor feature formed from serpentinization-related seepage from shallow-marine settings.

Today, the Semail Ophiolite is host to numerous terrestrial hyperalkaline springs, the famous Omani ‘Blue Pools’ (e.g. Neal & Stanger, 1984; Chavagnac *et al.* 2013; Giampouras *et al.* 2020), where serpentinization-derived fluids mix with meteoric waters. Earlier evidence of serpentinization of the Semail Ophiolite comes from Wadi Fins in SE Oman where there are veins of calcite and subordinate dolomite within a host rock of serpentinized peridotite, associated with deep clastic dykes filled with sedimentary carbonates (de Obeso & Kelemen, 2018, 2020; Cooperdock *et al.* 2020). These calcite veins have  $^{87}\text{Sr}/^{86}\text{Sr}$  ratios indicative of an age around the Cretaceous–Paleocene boundary (de Obeso & Kelemen, 2018) and (U–Th)/He values in hydrothermal magnetite in the veins, which give an age estimate of  $15 \pm 4$  Ma, equating to the Miocene (Cooperdock *et al.* 2020). Cooperdock *et al.* (2020) interpreted these calcite veins as having formed over a considerable period of time through the interaction of the Semail Ophiolite mantle peridotites with pore fluids derived from overlying Cretaceous and Paleocene limestone formations. The JHM shows that similar processes started earlier, possibly in late Campanian to early Maastrichtian time, soon after the end of ophiolite obduction onto the Arabian continental margin (Searle & Cox, 1999). Post-emplacement serpentinization of the Semail Ophiolite likely occurred even before this, as lateritic debris in conglomerates at the base of Maastrichtian marine sediments show that parts of the ophiolite were raised above sea-level prior to the early Maastrichtian transgression and subjected to sub-aerial weathering

(Coleman, 1981; Al-Khribash, 2015). It seems likely that some serpentinization could have occurred during this weathering phase. Further, based on  $\delta^{18}\text{O}$  data Gregory & Taylor (1981) suggested that some serpentinization of the Semail Ophiolite mantle sequence was taking place even as it was being formed. The reconstructed composition of the JHM fluids differs from the modern Semail Ophiolite hyperalkaline springs in being a mixture of serpentinization-derived fluids with seawater rather than with meteoric waters and the precipitation of calcite only, rather than calcite, aragonite and brucite. Because brucite is retro-soluble, it is conceivable that this mineral was precipitated during the formation of the JHM and was then replaced during diagenesis. However, there is no petrological evidence (e.g. pseudomorphic minerals) in the studied JHM thin-sections for this sort of replacement process. Further, brucite has not been recorded in the Wadi Fins calcite veins, which de Obeso & Kelemen (2018) interpreted as an indication of non-isochemical serpentinization at that site. The JHM calcite cement  $\delta^{13}\text{C}$  values are more negative than those from the Wadi Fins calcite veins ( $-1.3$  to  $+0.6$  ‰), which correspond rather to the values from the overlying Simsim Formation (de Obeso & Kelemen, 2018).

Close modern analogues to the environment in which the JHM formed are the shallow-marine serpentinization-derived fluid and gas seeps found in the Bay of Prony, New Caledonia and off the island of Elba, Italy. The Prony hydrothermal field (PHF) comprises a suite of fluid seeps in a marine lagoon, in the intertidal zone and onshore springs (Launay & Fontes, 1985; Monnin *et al.* 2014; Pisapia *et al.* 2017). The marine seeps are precipitating submarine carbonate structures with complex morphologies in the 30 m and 50 m depth range, including the well-known Aiguille de Prony, which is 35 m tall and reaches to within 2 m of the water surface. These structures are highly porous and are formed largely of calcite, with increasing amounts of brucite mixed with Mg-carbonates and aragonite towards their interiors (Pisapia *et al.* 2017). The PHF fluids have a high pH and high concentration of aqueous calcium and hydroxide, with only traces of other solutes (Monnin *et al.* 2014). The low salinity values agree with fluids derived from the mixing of meteoric water with fluids derived from serpentinization, even though in most places in the Bay of Prony fluids are now discharging into the sea and ultimately mix with seawater. In this respect they differ from the composition of the fluids which formed the JHM, which we infer to have had a large seawater component, at least for the early cement phase.

Another analogous modern setting to the JHM are sites offshore Elba in the Tyrrhenian Sea (Meister *et al.* 2018; Sciarra *et al.* 2019). At the Pomonte site, gas emission occurs across an area of 1000 m<sup>2</sup> of seafloor in 10–13 m water depth through quartz-rich, organic-poor sands, deposited on top of rocks of the Ligurian Ophiolite, which locally include serpentinized peridotite. Gas bubbles are enriched in methane ( $\delta^{13}\text{C}_{\text{methane}} \sim -18$  ‰) and hydrogen, and have a very low CO<sub>2</sub> content. The gas seeps are associated with areas of discoloured sediment containing semi-lithified carbonate crusts, at between 20 and 40 cm depth within the sediment. The crusts are formed of spherulitic, fibrous aragonite that cements sand grains and sometimes bryozoans and seagrass rhizome fibres. The crusts have  $\delta^{13}\text{C}$  values of between  $-17$  and  $+2$  ‰ and  $\delta^{18}\text{O}$  values of approximately  $+1.5$  ‰. Based on the decrease in pore water sulphate concentrations at the gas seeps relative to seawater, increases in sulphide and DIC, and the negative  $\delta^{13}\text{C}$  values, Meister *et al.* (2018) inferred that the Elba seep carbonate cements are the product of microbial sulphate-dependent anaerobic oxidation of abiotic methane (AOM).

This scenario of AOM-related carbonate precipitation in shallow-marine sediments can be applied to the hardgrounds in the Qahlah Formation, although the  $\delta^{13}\text{C}$  values of the latter are more positive than some of the Elba seep carbonate values. The JHM itself contrasts with the Elba example because the carbonates are calcite rather than aragonite, which may reflect the predominantly calcite precipitation in Cretaceous seas (Sandberg, 1983), rather than any fundamental differences in seepage fluid composition. Other differences are that the JHM shows evidence of several stages of fluid mixing and cement precipitation to form seafloor rather than subsurface features as in Elba. Nonetheless, there are enough similarities between the New Caledonian and Elba examples and the JHM to indicate the latter (and possibly the Qahlah Formation hardgrounds) is another example of shallow-marine serpentinite-derived seepage, and therefore adds a data point in the geological record to our knowledge of this interesting phenomenon.

**Acknowledgements.** We thank Sebastian Flotow (Bremen) for the preparation of petrographic thin-sections and Heike Anders (Bremen) for help and assistance with LA-ICP-MS analyses. Mark Wilson (Wooster) is thanked by P.D.T. for his help during fieldwork. This work was supported by the Deutsche Forschungsgemeinschaft (B.E., grant number 5441317) and a Fellowship from the Hanse-Wissenschaftskolleg (HWK) to C.T.S.L. to support visits to the University of Bremen. Comments by Bas van de Schootbrugge and an anonymous reviewer are gratefully acknowledged.

**Supplementary material.** To view supplementary material for this article, please visit <https://doi.org/10.1017/S0016756821000121>

## References

- Abbasi IA, Hersi OS and Al-Harthy A (2014) Late Cretaceous conglomerates of the Qahlah Formation, north Oman. In *Tectonic Evolution of the Oman Mountains* (eds HR Rollinson, MP Searle, IA Abbasi, A Al-Lazki and MH Al Kindi), pp. 325–41. Geological Society of London, Special Publication no. 392.
- Abdelghany O (2006) Early Maastrichtian larger foraminifera of the Qahlah Formation, United Arab Emirates and Sultanate of Oman borders. *Cretaceous Research* 27, 898–906.
- Abrajano TA, Sturchio NC, Bohlke JK, Lyon GL, Poreda RJ and Stevens CM (1988) Methane-hydrogen gas seeps, Zambales ophiolite, Philippines: deep or shallow origin? *Chemical Geology* 71, 211–22.
- Abrajano TA, Sturchio NC, Kennedy BM, Lyon GL, Muehlenbachs K and Bohlke JK (1990) Geochemistry of reduced gas related to serpentinization of the Zambales ophiolite, Philippines. *Applied Geochemistry* 5, 625–30.
- Agrinier P, Cornen G and Beslier M-O (1996) Mineralogical and oxygen isotopic features of serpentinites recovered from the ocean/continent transition in the Iberia abyssal plain. In *Proceedings of the Ocean Drilling Program, Scientific Results, vol. 149* (eds RB Whitmarsh, DS Sawyer, A Klaus and DG Masson), pp. 541–52. College Station, Texas.
- Al-Khribash S (2015) Genesis and mineralogical classification of Ni-laterites, Oman Mountains. *Ore Geology Reviews* 65, 199–212.
- Alsens H, Regnery J, Ashckenazi-Polivoda S, Meilijson A, Ron-Yankovich L, Abramovich S, Illner P, Almogi-Labin A, Feinstein S, Berner Z and Püttmann W (2013) Sea surface temperature record of a Late Cretaceous tropical southern Tethys upwelling system. *Palaeogeography, Palaeoclimatology, Palaeoecology* 392, 350–8.
- Alsharan AS and Nasir SJY (1996) Sedimentological and geochemical interpretation of a transgressive sequence: the Late Cretaceous Qahlah Formation in the western Oman Mountains, United Arab Emirates. *Sedimentary Geology* 101, 227–42.
- Bach W, Paulick H, Garrido CJ, Ildefonse B, Meurer WP and Humphris SE (2006) Unraveling the sequence of serpentinization reactions: petrography, mineral chemistry, and petrophysics of serpentinites from MAR 15°N (ODP

- Leg 209, Site 1274). *Geophysical Research Letters* **33**, L13306. doi: [10.1029/2006GL025681](https://doi.org/10.1029/2006GL025681).
- Blank JG, Green SJ, Blake D, Valley JW, Kita NT, Treiman A and Dobson PF** (2009) An alkaline spring system within the Del Puerto Ophiolite (California, USA): a Mars analog site. *Planetary and Space Science* **57**, 533–40.
- Bromley RG** (1996) *Trace Fossils. Biology, Taphonomy and Applications*. London: Chapman and Hall, 361 pp.
- Bruni J, Canepa M, Chiodini G, Cioni R, Cipolli F, Longinelli A, Marini L, Ottonello G and Zuccolini MV** (2002) Irreversible water-rock mass transfer accompanying the generation of the neutral, Mg–HCO<sub>3</sub> and high-pH, Ca–OH spring waters of the Genova province, Italy. *Applied Geochemistry* **17**, 455–74.
- Buggisch W and Krumm S** (2005) Palaeozoic cold seep carbonates from Europe and North Africa – an integrated isotopic and geochemical approach. *Facies* **51**, 566–83.
- Charlou LL, Donval JP, Fouquet Y, Jean-Baptiste P and Holm N** (2002) Geochemistry of high H<sub>2</sub> and CH<sub>4</sub> vent fluids issuing from ultramafic rocks at the Rainbow hydrothermal field (36°14'N, MAR). *Chemical Geology* **191**, 345–59.
- Chavagnac V, Monnin C, Ceuleneer G, Boulart C and Hoareau G** (2013) Characterization of hyperalkaline fluids produced by low-temperature serpentinization of mantle peridotites in the Oman and Ligurian ophiolites. *Geochemistry, Geophysics, Geosystems* **14**, 2496–522.
- Coggon RM, Teagle DAH, Smith-Duque CE, Alt JC and Cooper MJ** (2010) Reconstructing past seawater Mg/Ca and Sr/Ca from mid-ocean ridge flank calcium carbonate veins. *Science* **327**, 1114–17.
- Coleman RG** (1981) Tectonic setting for ophiolite obduction in Oman. *Journal of Geophysical Research* **86**, 2497–508.
- Cooperdock EHG, Stockli DF, Kelemen PB and de Obeso JC** (2020) Timing of magnetite growth associated with peridotite-hosted carbonate veins in the SE Samail ophiolite, Wadi Fins, Oman. *Journal of Geophysical Research: Solid Earth* **125**, e2019JB018632. doi: [10.1029/2019JB018632](https://doi.org/10.1029/2019JB018632).
- Craig H** (1957) Isotopic standards for carbon and oxygen and correction factors for mass-spectrometric analysis of carbon dioxide. *Geochimica et Cosmochimica Acta* **12**, 133–49.
- de Obeso JC and Kelemen PB** (2018) Fluid rock interactions on residual mantle peridotites overlain by shallow oceanic limestones: insights from Wadi Fins, Sultanate of Oman. *Chemical Geology* **498**, 139–49.
- de Obeso JC and Kelemen PB** (2020) Major element mobility during serpentinization, oxidation and weathering of mantle peridotite at low temperatures. *Philosophical Transactions of the Royal Society A*, **378**, 20180433. doi: [10.1098/rsta.2018.0433](https://doi.org/10.1098/rsta.2018.0433).
- Eickmann B, Bach W, Rosner M and Peckmann J** (2009) Geochemical constraints on the modes of carbonate precipitation in peridotites from the Logatchev hydrothermal vent field and Gakkel ridge. *Chemical Geology* **268**, 97–106.
- Eickmann B, Thorseth IH, Peters M, Strauss H, Bröcker M and Pedersen RB** (2014) Barite in hydrothermal environments as a recorder of sub-seafloor processes. *Geobiology* **12**, 308–21.
- Erhardt AM, Turchyn AV, Dickson JAD, Sadekov AY, Taylor PD, Wilson MA, Scott P and Schrag DP** (2020) Chemical composition of carbonate hardground cements as reconstructive tools for Phanerozoic pore fluids. *Geochemistry, Geophysics, Geosystems* **21**, e2019GC008448. doi: [10.1029/2019GC008448](https://doi.org/10.1029/2019GC008448).
- Etiopie G, Schoell M and Hosgormez H** (2011) Abiotic methane flux from the Chimaera seep and Tekirova ophiolites (Turkey): understanding gas exhalation from low temperature serpentinization and implications for Mars. *Earth and Planetary Science Letters* **310**, 96–104.
- Friedmann L and O'Neil JR** (1977) Compilation of stable isotope fractionation factors of geochemical interest. In *Data of Geochemistry, 6th Edition* (ed. M Fleischer), pp. 1–117. US Geological Survey Professional Paper no. 440.
- Früh-Green GL, Kelley DS, Bernasconi SM, Karson JA, Ludwig KA, Butterfield DA, Boschi C and Proskurowski G** (2003) 30,000 years of hydrothermal activity at the Lost City vent field. *Science* **301**, 495–8.
- Fryer P, Ambos EL and Hussong DM** (1985) Origin and emplacement of Mariana forearc seamounts. *Geology* **13**, 774–7.
- Giampouras M, Garrido CJ, Bach W, Los C, Fussmann D, Monien P and García-Ruiz JM** (2020) On the controls of mineral assemblages and textures in alkaline springs, Samail Ophiolite, Oman. *Chemical Geology* **533**, 119435. doi: [10.1016/j.chemgeo.2019.119435](https://doi.org/10.1016/j.chemgeo.2019.119435).
- Glennie KW, Boeuf MGA, Clarke MH, Moody-Stuart M, Pilaar WFH and Reinhardt BM** (1973) Late Cretaceous nappes in Oman Mountains and their geologic evolution. *American Association of Petroleum Geologists Bulletin* **57**, 5–27.
- Gregory MR, Martin AJ and Campbell KA** (2004) Compound trace fossils formed by plant and animal interactions: Quaternary of northern New Zealand and Sapelo Island, Georgia (USA). *Fossils and Strata* **51**, 88–105.
- Gregory RT and Taylor HP** (1981) An oxygen isotope profile in a section of Cretaceous oceanic crust, Samail ophiolite, Oman: evidence for δ<sup>18</sup>O buffering of the oceans by deep (>5 km) seawater–hydrothermal circulation at mid-ocean ridges. *Journal of Geophysical Research* **86**, 2737–55.
- Hardie LA** (1996) Secular variations in seawater chemistry: an explanation for the coupled secular variation in the mineralogies of marine limestones and potash evaporates over the past 600 m.y. *Geology* **24**, 279–83.
- Irwin H, Curtis C and Coleman M** (1977) Isotopic evidence for source of diagenetic carbonates formed during burial of organic-rich sediments. *Nature* **269**, 209–13.
- Joseph C, Campbell KA, Torres ME, Martin RA, Pohlman JW, Riedel M and Rose K** (2013) Methane-derived authigenic carbonates from modern and paleoseeps on the Cascadia margin: mechanisms of formation and diagenetic signals. *Palaeogeography, Palaeoclimatology, Palaeoecology* **390**, 52–67.
- Kelley DS, Karson JA, Blackman DK, Früh-Green GL, Butterfield DA, Lilley MD, Olson EJ, Schrenk MO, Roe KK, Lebon GT, Rivizzigno P and the AT3-60 Shipboard Party** (2001) An off-axis hydrothermal vent field near the Mid-Atlantic Ridge at 30°N. *Nature* **412**, 145–9.
- Kim S-T and O'Neil JR** (1997) Equilibrium and nonequilibrium oxygen isotope effects in synthetic carbonates. *Geochimica et Cosmochimica Acta*, **61**, 3461–75.
- Klein F, Humphris SE, Guo W, Schubotz F, Schwarzenbach EM and Orsi WD** (2015) Fluid mixing and the deep biosphere of a fossil Lost City-type hydrothermal system at the Iberia Margin. *Proceedings of the National Academy of Sciences of the United States of America* **112**, 12036–41.
- Lafay R, Baumgartner LP, Schwartz S, Picazo S, Montes-Hernandez G and Vennemann T** (2017) Petrologic and stable isotopic studies of the fossil hydrothermal system in ultramafic environment (Chenailette ophiolites, Western Alps, France): processes of carbonate cementation. *Lithos* **294–295**, 319–38.
- Lang SQ, Butterfield DA, Schulte M, Kelley DS and Lilley MD** (2010) Elevated concentrations of formate, acetate and dissolved organic carbon found at the Lost City hydrothermal field. *Geochimica et Cosmochimica Acta* **74**, 941–52.
- Launay J and Fontes JC** (1985) Les sources thermals de Prony (Nouvelle-Calédonie) et leurs précipités chimiques. Exemple de formation de brucite primaire. *Géologie de la France* **1**, 83–100.
- Lavoie D and Chi G** (2010) An Ordovician “Lost City” — venting serpentinite and life oases on Iapetus seafloor. *Canadian Journal of Earth Sciences* **47**, 199–207.
- Lilley MD, Butterfield DA, Olson EJ, Lupton JE, Macko SA and McDuff RE** (1993) Anomalous CH<sub>4</sub> and NH<sub>4</sub><sup>+</sup> concentrations at an unsedimented mid-ocean-ridge hydrothermal system. *Nature* **364**, 45–7.
- Ludwig KL, Kelley DS, Butterfield DA, Nelson BK and Früh-Green G** (2006) Formation and evolution of carbonate chimneys at the Lost City Hydrothermal Field. *Geochimica et Cosmochimica Acta* **70**, 3625–45.
- Meister P, Wiedling J, Lott C, Bach W, Kuhfuß H, Wegener G, Böttcher ME, Deusner C, Lichtschlag A, Bernasconi SM and Weber M** (2018) Anaerobic methane oxidation inducing carbonate precipitation at abiogenic methane seeps in the Tuscan archipelago (Italy). *PLoS One* **13**, e0207305. doi: [10.1371/journal.pone.0207305](https://doi.org/10.1371/journal.pone.0207305).
- Monnin C, Chavagnac V, Boulart C, Ménez B, Gérard M, Gérard E, Pisapia C, Quéméneur M, Erauso G, Postec A, Guentas-Dombrowski L, Payri C and Pelletier B** (2014) The low temperature hyperalkaline hydrothermal system of the Prony Bay (New Caledonia). *Biogeosciences* **11**, 6221–67.
- Muehlenbachs K** (1998) The oxygen isotopic of the oceans, sediments and the seafloor. *Chemical Geology* **145**, 263–73.
- Neal C and Stanger G** (1984) Calcium and magnesium hydroxide precipitation from alkaline groundwaters in Oman, and their significance to the process of serpentinization. *Mineralogical Magazine* **48**, 237–41.
- Palandri JL and Reed MH** (2004) Geochemical models of metasomatism in ultramafic systems: serpentinization, rodingitization, and sea floor carbonate chimney precipitation. *Geochimica et Cosmochimica Acta* **68**, 1115–33.

- Pearce NJG, Perkins WT, Westgate JA, Gorton MP, Jackson SE, Neal CR and Chenery SP (1997) A compilation of new and published major and trace element data for NIST SRM 610 and NIST SRM 612 Glass Reference Materials. *Geostandards Newsletter* **21**, 115–44.
- Pearson PN, Ditchfield PW, Singano J, Harcourt-Brown KG, Nicholas CJ, Olsson RK, Shackleton NJ and Hall MA (2001) Warm tropical sea surface temperatures in the Late Cretaceous and Eocene epochs. *Nature* **413**, 481–7.
- Peckmann J, Campbell KA, Walliser OH and Reitner J (2007) A Late Devonian hydrocarbon-seep deposit dominated by dimerelloid brachiopods, Morocco. *Palaaios* **22**, 114–22.
- Pisapia C, Gérard E, Gérard M, Lecourt L, Lang SQ, Pelletier B, Payri CE, Monnin C, Guentas L, Postec A, Quéméneur M, Erauso G and Ménez B (2017) Mineralizing filamentous bacteria from the Prony Bay Hydrothermal Field give new insights into the functioning of serpentinization-based seafloor ecosystems. *Frontiers in Microbiology* **8**, 57. doi: [10.3389/fmicb.2017.00057](https://doi.org/10.3389/fmicb.2017.00057).
- Prokoph A, Shields GA and Veizer J (2008) Compilation and time-series analysis of a marine carbonate  $\delta^{18}\text{O}$ ,  $\delta^{13}\text{C}$ ,  $^{87}\text{Sr}/^{86}\text{Sr}$  and  $\delta^{34}\text{S}$  database through Earth history. *Earth-Science Reviews* **87**, 113–33.
- Proskurowski G, Lilley MD, Seewald JS, Früh-Green GL, Olson EJ, Lupton JE, Sylva SP and Kelley DS (2008) Abiogenic hydrocarbon production at Lost City Hydrothermal Field. *Science* **319**, 604–7.
- Rausch S, Bohm F, Bach W, Klügel A and Eisenhauer A (2013) Calcium carbonate veins in ocean crust record a threefold increase of seawater Mg/Ca in the past 30 million years. *Earth and Planetary Science Letters* **362**, 215–24.
- Rimstidt JD, Balog A and Webb J (1998) Distribution of trace elements between carbonate minerals and aqueous solutions. *Geochimica et Cosmochimica Acta* **62**, 1851–63.
- Sandberg PA (1983) An oscillating trend in Phanerozoic non-skeletal carbonate mineralogy. *Nature* **305**, 19–22.
- Schlüter M, Steuber T, Parente M and Mutterlose J (2008) Evolution of a Maastrichtian–Paleocene tropical shallow-water carbonate platform (Qalhat, NE Oman). *Facies* **54**, 513–27.
- Sciarrà A, Saroni A, Etiope G, Coltorti M, Mazzarini F, Lott C, Grassa F and Italiano F (2019) Shallow submarine seep of abiogenic methane from serpentinized peridotite off the Island of Elba, Italy. *Applied Geochemistry* **100**, 1–7.
- Searle M and Cox J (1999) Tectonic setting, origin and obduction of the Oman ophiolite. *Geological Society of America Bulletin* **111**, 102–22.
- Skelton PW, Nolan SC and Scott RW (1990) The Maastrichtian transgression onto the northwestern flank of the Proto-Oman Mountains: sequences of rudist-bearing beach to open shelf facies. In *The Geology and Tectonics of the Oman Region* (eds AHF Robertson, MP Searle and AC Ries), pp. 521–47. Geological Society of London, Special Publication no. 49.
- Sleep NH, Meibom A, Fridriksson T, Coleman RG and Bird DK (2004)  $\text{H}_2$ -rich fluids from serpentinization: geochemical and biotic implications. *Proceedings of the National Academy of Sciences of the United States of America* **101**, 12818–23.
- Smith AB, Morris NJ, Gale AS and Kennedy WJ (1995) Late Cretaceous carbonate platform faunas of the United Arab Emirates–Oman border region. *Bulletin of The Natural History Museum, London, Geology Series* **51**, 91–119.
- Taylor SR and McLennan SM (1985) *The Continental Crust: Its Composition and Evolution*. Oxford: Blackwell Scientific Publications, 312 pp.
- Tong H, Wang Q, Peckmann J, Cao Y, Chen L, Zhou W and Chen D (2016) Diagenetic alteration affecting  $\delta^{18}\text{O}$ ,  $\delta^{13}\text{C}$  and  $^{87}\text{Sr}/^{86}\text{Sr}$  signatures of carbonates: a case study on Cretaceous seep deposits from Yarlung-Zangbo Suture Zone, Tibet, China. *Chemical Geology* **444**, 71–82.
- Tucker ME and Wright PV (1990) *Carbonate Sedimentology*. Oxford: Blackwell Science.
- Veizer J, Bruckschen P, Pawelick F, Diener A, Podlaha OG, Carden GAF, Jasper T, Korte C, Strauss H, Azmy K and Ala D (1997) Oxygen isotope evolution of Phanerozoic seawater. *Palaeoogeography* **132**, 159–72.
- Wallmann K (2001) Controls on the Cretaceous and Cenozoic evolution of seawater composition, atmospheric  $\text{CO}_2$  and climate. *Geochimica et Cosmochimica Acta* **65**, 3005–25.
- Wilson PA and Opdyke BN (1996) Equatorial sea-surface temperatures for the Maastrichtian revealed through remarkable preservation of metastable carbonate. *Geology* **24**, 555–8.
- Wilson MA and Taylor PD (2001) Palaeoecology of hard substrate faunas from the Cretaceous Qalhat Formation of the Oman Mountains. *Palaentology* **44**, 21–41.
- Zeebe RE (2001) Seawater pH and isotopic paleotemperatures of Cretaceous oceans. *Palaeoogeography, Palaeoclimatology, Palaeoecology* **170**, 49–57.
- Zeebe RE and Wolf-Gladrow D (2001)  *$\text{CO}_2$  in Seawater: Equilibrium, Kinetics, Isotopes*. Elsevier Oceanography Series 65. Amsterdam: Elsevier.